Streptococcus mutans yidC1 and *yidC2* impact cell-envelope biogenesis, biofilm matrix and biophysical properties

Sara R. Palmer[1#], Zhi Ren[2,3], Geelsu Hwang[2], Yuan Liu[2], Ashton Combs[1], Bill Söderström [4], Patricia Lara Vasquez [5], Yalda Khosravi[6], L. Jeannine Brady[5#], Hyun Koo[2], and Paul Stoodley,[6,7,8]

Division of Biosciences, College of Dentistry, The Ohio State University, Columbus, Ohio, USA[1]

Biofilm Research Labs, Levy Center for Oral Health, Department of Orthodontics and Divisions of Pediatric Dentistry and Community of Oral Health, University of Pennsylvania, Philadelphia, Pennsylvania, USA[2]

State Key Laboratory of Oral Diseases, West China School of Stomatology, Sichuan University, Chengdu, China[3]

Structural Cellular Biology Unit, Okinawa Institute of Science and Technology, Okinawa, Japan[4]

Department of Oral Biology, College of Dentistry, University of Florida, Gainesville, Florida, USA[5]

Department of Microbial Infection and Immunity, College of Medicine, The Ohio State University, Columbus, Ohio, USA[6]

Department of Orthopedics, College of Medicine, The Ohio State University, Columbus, Ohio, USA[7]

National Centre for Advanced Tribology at Southampton (nCATS), Dept. Mechanical Engineering University of Southampton, UK[8]

Running title: *S. mutans* YidCs contribute to biofilm development

Address correspondence to L. Jeannine Brady jbrady@dental.ufl.edu or Sara Palmer palmer.750@osu.edu

Abstract

Proper envelope biogenesis of *Streptococcus mutans,* a biofilm-forming and dental caries causing oral pathogen*,* requires two paralogs (*yidC1* and *yidC2*) of the universally conserved YidC/Oxa1/Alb3 family of membrane integral chaperones and insertases. Deletion of either paralog attenuates virulence *in vivo* but the mechanisms of disruption remain unclear. Here, we determined whether deletion of *yidC* affects cell surface properties, extracellular glucan production, and/or the structural organization of EPS matrix and biophysical properties of *S. mutans* biofilm. Compared to wild type, the *ΔyidC*2 mutant lacked staining with vancomycin at the division septum, while the *ΔyidC1* mutant resembled wild-type. Additionally, deletion of either *yidC1* or *yidC2* resulted in less insoluble glucan synthesis, but produced more soluble glucans, especially at early and mid-exponential growth phases. Alteration of glucan synthesis by both mutants yielded biofilms with less dry-weight and insoluble EPS. In particular, deletion of *yidC2* resulted in significant reduction of biofilm biomass and pronounced defects in the spatial organization of the EPS matrix, thus modifying the 3D biofilm

architecture. The defective biofilm harbored smaller bacterial clusters with high cell density and less surrounding EPS compared to wild type, which was stiffer in compression yet more susceptible to removal by shear. Together, our results indicate that elimination of either *yidC* paralog results in changes to the cell envelope and glucan production that ultimately disrupts biofilm development and EPS matrix structure-composition, thereby altering the physical properties of the biofilms and facilitating their removal. YidC proteins, therefore, represent potential therapeutic targets for cariogenic biofilm control.

Importance. YidC proteins are membrane localized chaperone insertases that are universally conserved in all bacteria, and are traditionally studied in the context of membrane protein insertion and assembly. Both YidC paralogs of the cariogenic pathogen *Streptococcus mutans* are required for proper envelope biogenesis and full virulence, indicating these proteins may also contribute to optimal biofilm formation in streptococci. Here we show that deletion of either *yidC* results in changes to the structure and physical properties of the EPS matrix produced by *S. mutans*, ultimately impairing optimal biofilm development, diminishing its mechanical stability, and facilitating its removal. Importantly, the universal conservation of bacterial *yidC* orthologs, combined with our findings, provide a rationale for YidC as a possible drug target for anti-biofilm therapies.

Introduction

Streptococcus mutans resides primarily in biofilms formed on tooth surfaces (termed dental plaque), often leading to dental caries, a prevalent and costly oral

disease that causes damage (cavitation) to the mineralized tissue (1-3). While, *S. mutans* is a minor component of the total bacterial community in healthy conditions (4), this opportunistic pathogen can rapidly assemble virulent biofilms via production of extracellular polysaccharides (EPS) when conditions are conducive to dental caries, i.e. high exposure to dietary sugars (5, 6). *S. mutans* secretes glucosyltransferase exoenzymes (Gtfs), which can bind to both tooth and microbial surfaces, as well as promote bacterial accumulation and EPS-rich matrix assembly (5). When sucrose becomes increasingly available, insoluble glucans produced by *S. mutans'* Gtf enzymes embed the bacterial cells in a polymeric matrix that enhances adhesion-cohesion and creates diffusion-limiting milieus, thereby fundamentally changing the architecture and physical properties of the dental plaque biofilm (6). The metabolic activity of the microorganisms within the matrix can result in the formation of acidic and anaerobic microenvironments (6, 7), which progressively shift the bacterial community to one enriched in acidogenic and acid tolerant species (8). If biofilm persists, the acidification of the microenvironment at the tooth-biofilm interface ultimately results in acid-dissolution of the adjacent enamel, causing the onset of cavitation (3). Thus, the composition of the EPS matrix can both impact biofilm formation and accumulation, and create a pathogenic niche in close proximity of the tooth surface.

As with many Gram-positive bacterial pathogens, the majority of *S. mutans* virulence factors are either secreted, attached to the cell-wall, or located in the cytoplasmic membrane (9); this includes the membrane-associated glucan binding proteins (Gbp) and the secreted glycosyltransferases (Gtf) required for cariogenic biofilm formation (10). During bacterial protein translocation, best characterized in

Escherichia coli, proteins with N-terminal signal sequences destined for either insertion into or secretion across the cytoplasmic membrane are targeted to the SecYEG translocon (reviewed in (11, 12)). While many components of protein translocation pathways are universally conserved, there are differences in the accessory components and essentiality among bacterial species (12-15). The signal recognition particle (SRP), SecYEG, and YidC are found in all Bacteria, Archaea and eukaryotic organelles; however, streptococci do not have SecB, SecD or SecF and harbor two YidC paralogues of the universally conserved YidC/Oxa1/Alb3 protein family found in bacteria, mitochondria, and chloroplasts (16-19). *E. coli* and other Gram-negative organisms possess one *yidC;* whereas almost all Gram-positive organisms possess two or more (20).

Bacterial YidC proteins function as membrane integral chaperone/insertases, which insert membrane proteins into the lipid bilayer in conjunction with the SecYEG translocon (sec-dependent pathway) (21) and/or the signal recognition particle (SRP) co-translational protein translocation pathway (22). In the case of a few small single transmembrane domain hydrophobic proteins, a Sec-independent YidC only pathway is sufficient for membrane insertion (23). There is growing evidence that YidC proteins may also impact cell surface biogenesis and maturation of secreted proteins (24-26). *Staphylococcus aureus* YidC was recently identified as a target of a compound capable of inhibiting biofilm formation and reducing virulence (27).

The two YidC paralogs of *S. mutans* are 27% identical and 48% similar based on protein sequence (EMBOSS Needle, EBlosum62). Each is predicted to contain five transmembrane domains after processing and removal of their signal peptides by

SPaseII (28). While there are a number of conserved residues within the transmembrane domains of bacterial YidC proteins (29), the cytoplamsically located C-terminal tails of *S. mutans* YidC1 and YidC2 differ in both length and charge. Similarly, the length and charge distribution of residues within the two cytoplasmic loops, that in *Bacillus halodurans* interact to form what is known as the C1 domain (30), differ between *S. mutans* YidC1 and YidC2. It has been reported that, the C-terminal tail of either *S. mutans* YidC protein can facilitate interactions with translating ribosomes in a heterologous *E. coli* system, possibly allowing for co-translational translocation (31) and explaining why elimination of the universally conserved co-translational SRP pathway is dispensable in *S. mutans* (16). Both YidC proteins appear to be constitutively expressed in *S. mutans;* however, *yidC2* expression also appears to be influenced by the LiaFSR three-component system (Palmer et al, unpublished) that senses and responds to cell envelope stress (32).

Deletion of *E. coli yidC* is lethal (33), as is simultaneous deletion of *yidC1* and *yidC2* in *S. mutans* (25). Single deletion of *yidC1* has little apparent effect on growth or stress tolerance, whereas disruption of *yidC2* results in a pronounced stress-sensitive phenotype (acid, osmotic, and oxidative) similar to disruption of the SRP pathway (16, 25). In experiments in which DNA encoding the C-terminal tails of *yidC1* and *yidC2* were exchanged to generate chimeric proteins, the *yidC1-C2* chimeric construct partially restored stress tolerance to the *ΔyidC2* mutant. In contrast, when DNA encoding the C-terminal tail of YidC1 replaced that of *yidC2* (*yidC2-C1*), a dominant negative effect on growth and protein secretion was observed (25). These results highlight the functional

differences between *S. mutans* YidC1 and YidC2 and demonstrate that differences in their C-terminal tails are at least partially responsible for their respective functions.

Despite substantial phenotypic differences between *yidC1* and *yidC2* deletion strains observed in *in vitro* studies, both mutants are attenuated for virulence in a rat model of dental caries (25). Thus under *in* vivo conditions conducive to disease (high sucrose diet), both *S. mutans yidC* paralogs are required for full virulence. Therefore, defects in cell membrane and cell surface biogenesis stemming from elimination of *yidC1* or *yidC2* might also impact the ability of *S. mutans* to produce insoluble glucans that are critical for extracellular matrix assembly and biofilm formation under cariogenic conditions. The present study combines microscopy and biophysical-biochemical techniques to evaluate the consequences of *yidC1* and *yidC2* deletion on cell morphology and glucan synthesis in *S. mutans*, and evaluates the respective contribution of YidC1 and YidC2 to biofilm formation, structural integrity and EPS matrix production.

Results

yidC mutants have aberrant cell morphology, display defects in division septa, and cell wall characteristics.

While the Δ*yidC1* mutant's growth rate in planktonic culture is very similar to that of wild type, the Δ*yidC2* mutant has a reduced growth rate and self-aggregates. In the present study, the cell morphology of planktonically grown cells was compared by Gram-stain. Representative images of Gram-stained cells are shown in Figure 1A. We observed typical cell morphology for *S. mutans* in the wild type and Δ*yidC1* mutant, with

cells forming either pairs or longer chains. However, the Δ*yidC2* mutant cells formed large clumps, and made fewer and shorter chains. In addition, the Δ*yidC2* mutant cells were surrounded by a material that stained light pink, which could be cytoplasmic content (i.e. genomic DNA) that bound the safranin counterstain, potentially indicating the Δ*yidC2* mutant may lyse easier due to cell-wall or membrane defects.

In order to compare the details of the cell surface and cell-wall structures of the wild-type and mutant strains, scanning and transmission electron microscopy (SEM and TEM) were performed. By SEM, there were clear visual differences between the wild-type and *yidC* mutants, where both *yidC* mutant samples contained more cells with multiple division septa compared to wild-type (Figure 1B). In addition, there was asymmetry in the dividing cells in both *yidC* mutant samples, with multiple bowling pin shaped elongated cells evident (red arrows, Figure 1B and C). In addition, there was an absence of normally shaped ovococci, which were apparent in the wild type (yellow arrows, Figure 1B and C). To compare the internal cell structures, such as cell wall thickness and division septa, TEM was performed on ultra-thin (70 nm) sections from the wild-type and *yidC* mutant samples. Even at the lowest magnification (4,000 X), differences could be seen between wild-type and the *yidC* mutants, with multiple cross sections of elongated dividing cells present in the mutant samples (red arrows, Figure 2A). At 25,000 X and 60,000 X magnifications, normal dividing ovococci were apparent in the wild-type samples, while many asymmetrical dividing cells were present in the Δ*yidC1* and Δ*yidC2* mutant samples (red arrows, Figure 2B and 2C). Figure 2D shows a representative image at 100,000 X with visible cell walls from each strain. At this high magnification, differences in the quality of staining and presence of cell walls were

noticeable between the mutants and wild-type; the Δ*yidC2* mutant sample had fewer cells with intact cell walls, while the Δ*yidC1* mutant sample had more cells with intact cell walls compared to the wild-type sample.

Using calibrated micrograph images, cell wall thickness and cell diameter were measured using ImageJ (Figure 2E and F). The Δ*yidC2* mutant cells had significantly thinner cell walls ($P<0.013$) (Figure 2E) and the diameter of the Δ*yidC2* mutant cells were significantly larger compared to the wild-type (Figure 2F). The Δ*yidC1* mutant had similar cell wall thickness to the wild-type, but the staining of the cell walls with uranyl acetate was consistently more pronounced in the Δ*yidC1* mutant samples, which may suggest a higher protein content in the cell wall.

Given the differences in cell surface and cell wall characteristics observed for the *yidC* mutants, we also compared the *de novo* cell wall synthesis of each strain using fluorescently labeled vancomycin and super resolution Structured Illumination Microscopy (SIM). As shown in Figure 3, staining of the division septa of the Δ*yidC2* mutant was notably less pronounced than that observed for either the wild type or Δ*yidC1* strains, suggesting a potential defect in cell wall synthesis in the absence of *yidC2*. Consistant with TEM data, the Δ*yidC2* mutant cells were also significantly larger than those of the the wild-type when evlaluated by SIM (Figure 3D).

Glucan production by planktonic cultures of *yidC1/2* mutants differs from wild type and alters biofilm development.

To examine whether elimination of *S. mutans yidC1* and/or *yidC2* mutants might also affect extracellular proteins, we examined glycosyltransferase (Gtf) activity levels

since these are secreted enzymes in *S. mutans*. Using planktonic cultures, we compared the Gtf activity of culture supernatant collected from early-exponential, mid-exponential, and stationary phase cultures. Compared to the wild type parent, the Δ*yidC2* mutant produced significantly less insoluble and significantly more soluble glucan during all growth phases (Figure 4A and 4B). The effect of elimination of *yidC2* on soluble glucan production was most pronounced during early-exponential phase (Figure 4B). To verify that the change in insoluble/soluble glucan produced was due to the deletion of *yidC2* alone, a construct was generated in which a xylose inducible promoter controlled expression of *yidC2* (Supplemental Figure S1A). Therefore, *yidC2* was only expressed when xylose was present in the growth media (Supplemental Figure S1B). As shown in Figure 4C and 4D, behavior of the conditional expression strain grown with xylose resembled that of the wild type strain, whereas when grown without xylose the results paralleled those of the Δ*yidC2* deletion strain. In contrast to elimination of *yidC2*, elimination of *yidC1* had a more modest impact. Significantly less insoluble glucan was only observed for the Δ*yidC1* mutant compared to the wild type during early- and mid-exponential phases (Figure 4A). Significantly more soluble glucan production was only observed during the early-exponential phase for the Δ*yidC1* mutant compared to the wild type (Figure 4B).

To evaluate how the observed changes in secreted Gtf enzyme activity in the *yidC* mutants affect biofilm development, we compared the biomass (dry-weight) and the amount of extracellular polysaccharides between the biofilms formed by each *yidC* mutant and wild-type strain. The total biomass of a biofilm is a combination of bacterial cells, proteins and the constituents of the extracellular polysaccharides (EPS) matrix,

especially water-soluble and water-insoluble glucans (34). Both the Δ*yidC1* and Δ*yidC2* mutants formed biofilms with significantly less (33% and 48%, respectively) biomass (mg of total dry weight), compared to the wild type (Figure 5A). In addition, there were significant differences in the amounts and proportions of soluble and insoluble EPS. The Δ*yidC1* and Δ*yidC2* mutants both contained significantly less exopolysaccharides in their biofilms compared to wild type (Figure 5B). In particular, the Δ*yidC2* mutant biofilm showed a substantial reduction of insoluble EPS (>2.5 fold less than wild-type). In contrast, the Δ*yidC2* mutant biofilm harbored significantly more soluble EPS (Figure 5C). These results are consistent with the alterations in secreted Gtf activity observed for each glucan type (Figure 4).

The *yidC2* mutant biofilms contain smaller microcolonies and demonstrate a defective matrix.

Next, we wanted to determine how the changes in EPS composition by *yidC* mutants alter the biofilm structure and the extracellular matrix development. We compared the 3D architecture of biofilms formed by wild-type *S. mutans* to those of the Δ*yidC*1 or Δ*yidC2* mutants using confocal laser scanning microscopy (CLSM) and quantitative computational analysis as detailed previously (35). Figure 6A shows reconstructed renderings of biofilms of each of the *S. mutans* strains. Although only one representative image is presented for practicality, these analyses were performed in triplicate and at least 10 images were recorded under confocal microscopy. Consistent with biochemical data, we observed clear structural changes in the biofilm formed by the Δ*yidC2* mutant, which contained less and sparsely distributed EPS (red) compared to

252 the wild-type biofilm. Furthermore, orthogonal views (Figure 6A bottom) showed
253 reduced accumulation and thinner EPS, particularly at the upper layers of the Δ*yidC2*
254 mutant biofilm compared to the other two strains, indicating defective EPS-matrix
255 assembly. Interestingly, the biofilms formed between Δ*yidC1* mutant and wild type
256 appeared similar, despite the measured differences in their glucan content. The
257 biovolume of the EPS matrix from each biofilm quantified by COMSTAT revealed that
258 Δ*yidC2* mutant biofilms contained ~35 % less EPS (vs. intact *S. mutans* biofilm), while
259 Δ*yidC1* mutant biofilms harbored a similar amount. Additionally, the size of
260 microcolonies formed in the Δ*yidC2* mutant biofilm was significantly smaller compared
261 to wild-type biofilms (Figure 6B, $P < 0.05$), whereas no significant differences were
262 observed for the Δ*yidC1* mutant ($P > 0.05$). Similar results were observed when this
263 experiment was repeated using the complemented *yidC2* mutant strain in which *yidC2*
264 expression was controlled by a xylose inducible promoter, such that biofilms resembled
265 the wild-type parent strain when xylose was included in growth media, and resembled
266 the Δ*yidC2* mutant when xylose was not included (Figure 6A, inset).
267
268 **The Δ*yidC2* mutant produces stiffer biofilms that are more susceptible to shear**
269 In general, bacterial biofilms behave like viscoelastic fluids, which provide the
270 mechanical properties (adhesive and cohesive forces) (36, 37). Measuring the elastic
271 modulus (*E*) of a biofilm can reveal important differences about the cohesive forces
272 within the biofilm and can give an overall indication of global structural and physical
273 differences within the matrix. To understand how the changes in the biofilm structures
274 caused by Δ*yidC1* or Δ*yidC2* deletion affect the mechanical properties of *S. mutans*

biofilms, the elastic modulus was determined using an indentation/compression test (Figure 7A). The elastic modulus of each biofilm was calculated from the early, linear part of the force-displacement curve, where the geometry first came into contact with the biofilm (Figure 7A and B). The elastic modulus of the Δ*yidC2* mutant biofilms were significantly higher compared to wild-type biofilms (Figure 7C), indicating the Δ*yidC2* mutant formed more rigid biofilms. In addition, the Δ*yidC2* mutant formed thinner biofilms compared to wild type (Figure 7C). These results are consistent with the other changes observed in the Δ*yidC2* mutant biofilms, possibly due to differences in the ratio of soluble/insoluble glucans produced by this strain and in microcolony size. Further, the decrease in EPS matrix observed in the Δ*yidC2* mutant biofilms likely results in more tightly packed cells which could also help explain the distinct viscoelastic characteristic of this strain.

In addition, the mechanical stability of the biofilms was determined by measuring surface detachment of biofilm biomass exposed to shear stress. For these experiments the biofilms were exposed to 1.78 N/m^2 of shear stress for 10 min using a shear-induced biofilm mechanical strength tester (s-BMST) (Figure 8A) (38). The amount of biomass before and after the shear stress was determined by dry weight and confocal analysis (Figure 8B and C). The Δ*yidC2* mutant biofilm demonstrated the highest percentage of lost biomass (dry-weight) after shear stress, indicating weakened mechanical stability (Figure 8B). Likewise, quantitative imaging analysis using COMSTAT also revealed significantly less EPS and bacteria remaining after exposure to shear stress for the Δ*yidC2*, but not for the Δ*yidC1* mutant biofilm, compared to wild type (Figure 8C). These results are consistent with the reduced level of insoluble glucan

observed for the Δ*yidC2* mutant biofilm in that the level of insoluble glucan has been shown to be directly associated with biofilm attachment strength (28). However, mechanical strength was inversely proportional to the stiffness of the biofilm and was reflected in the higher elastic modulus of the Δ*yidC2* mutant biofilm compared to that of the wild type. These results imply that the amount and distribution of EPS could impact the biophysical properties of the biofilm and facilitate its removal.

Discussion

The phenotypic consequences of elimination of each of the two *S. mutans yidC* paralogs of the universally conserved YidC/Oxa1/Alb3 family differ (16, 39); however, we have found that proper surface biogenesis and attainment of characteristic virulence attributes of *S. mutans* depends to varying extents on both of these membrane-localized chareone insertases (25). Here we show that mutations in either *yidC1* or *yidC2* impact cell morphology and cell-wall properties of *S. mutans*, including alterations in septation and glucan production. These alterations, particularly those stemming from deletion of *yidC2,* have profound consequences for EPS matrix assembly-structure, thus impacting the biophysical properties and mechanical stability of the *S. mutans* biofilm. This new information furthers our understanding of how YidC1 and YidC2 contribute to cell physiology and development of cohesive and adherent biofilms that are associated with dental caries (6).

As determined by SEM, both *S. mutans yidC* mutants displayed aberrant cell shape and formed elongated cells. The effects were more pronounced in the *yidC2* mutant (Figure 1C). In *E.coli, yidC* depletion similarly resulted in aberrant cell

morphology, with cells forming longer bacilli compared to wild-type (24, 40). Although each of the *S. mutans* Δ*yidC1* and Δ*yidC2* mutants displayed differences in division septa frequency and cell shape in SEM experiments, only the Δ*yidC2* mutant demonstrated a clearly altered staining pattern when live cells were labeled with fluorescent vancomycin and imaged using super-resolution Structured Illumination Microscopy (SIM) microscopy (Figure 3). In this experiment, the Δ*yidC1* mutant resembled wild-type cells. Division-specific penicillin binding proteins such as PBP3 of *E. coli* or PBP2B and PBP1 of *Bacillus subtilis* localize at the division septum (41-43), hence the altered staining of the Δ*yidC2* mutant with the flourescent antibiotic suggests an underlying contribution of YidC2 to the cell wall biosynthesis machinery. In TEM experiments, the Δ*yidC2* mutant had measureably and significantly thinner cell-walls with larger cell diameter compared to wild-type parent. The lack of a punctate pattern at the division septa with a more peripheral cell wall staining with fluorescent vancomycin observed for the Δ*yidC2* mutant, was not shared by an *ffh* mutant (16) of *S. mutans*, which lacks the integral Ffh component of SRP pathway (data not shown). This finding is interesting since other phenotypic consequences are shared by the *yidC2* and *ffh* mutants of *S. mutans,* such as decreased mutacin production and genetic competence, as well as impaired tolerance to environmental stressors (16, 39). Double deletion mutants lacking both *yidC2* and *ffh* are not viable, suggesting a high degree of functional redundancy and cooperation between these protein translocation machinery components. Our current results indicate a clearcut instance in which YidC2 functions independently of the SRP pathway. In studies in *E. coli*, *yidC* depletion reduced the amount of the active form of penicillin binding proteins (PBPs), PBP2 and PBP3,

required for cell elongation and cell division, respectively, and the authors of that study concluded that YidC mediates folding of periplasmic domains of membrane proteins in *E. coli* (24). A PBP1a-deficient mutant of *S. mutans* resembles the *S. mutans yidC1* and *yidC2* mutants described herein (Figure 1), producing long rod-like cells with multiple division septa that are also defective in biofilm formation (44). Taken together, these results suggest that some of the phenotypic changes observed for the *S. mutans yidC* mutants could be due to improperly folded PBPs that would consequently affect cell division and morphology. Additional experiments are needed to further investigate potential compositional changes in the cell walls of the *yidC1* and *yidC2* mutants and to identify the respective substrates responsible for these alterations to identify the specific roles that *yidC1* and *yidC2* each apparently play in cell-wall development.

In addition to their roles in cell wall development and cell morphology, elimination of each *S. mutans yidC* paralog impacted secreted enzymatic actitivites causing significant alterations in extraceullular polysaccharide production (Figure 4). The effects of deletion of *yidC1* on soluble and insoluble EPS glucan production were modest and growth-phase dependent with no observable impact at stationary phase. In contrast, the consequences of elimination of *yidC2* were apparent during all growth phases and the decrease in insoluble glucans and increase in soluble glucans were far more pronounced than those observed in the Δ*yidC1* background. Insoluble glucan production is primarily associated with the enzymatic activity of the secreted GtfB exoenzyme, while GtfC produces a mixture of insoluble and soluble glucans (45). Because GtfBC activity is linked with EPS matrix assembly in cariogenic biofilms and manifestation of *S. mutans* virulence *in vivo* (5), the current data help to explain the

reduced levels of dental caries observed in rats infected with these mutants in a prior study (25). Although the entire spectrum of secretome and cell surface changes stemming from *yidC* mutations in *S. mutans* remains to be determined, both YidC1 and YidC2 may play important roles for secretion of Gtf exoenzymes. While YidC proteins are well known to function as membrane integral chaperone/insertases that are involved in the insertion and assembly of multimeric membrane proteins (20), the results presented here lend further support to the growing evidence that bacterial YidC's can also impact secreted proteins and cell-wall biogenesis (24-26).

Alterations in the physical properties of bacterial cells, such as changes in the cell-wall composition or charge distribution that influence surface properties, are known to affect biofilm formation (46). We observed that deletion of either *yidC1* or *yidC2* resulted in less overall biomass, with deviations in both the amount and type of EPS thus altering the 3D biofilm architecture. The Δ*yidC2* mutant strain produced less insoluble glucans and formed aberrant biofilms containing smaller cell clusters (or microcolonies) with sparser and thinner EPS-matrix compared to wild-type. These data are consistent with previous observations that insoluble glucans directly mediate the development and size of microcolonies (34, 35, 47). In contrast, the Δ*yidC1* mutant biofilms appeared similar to those of the wild type (Figure 6), despite measurable growth-phase dependent alterations observed in glucan production by culture supernatants derived from Δ*yidC1* strain (Figure 4). Previous studies have shown that a mutant lacking *gtfB* (insoluble glucan synthesis) was unable to develop EPS-microcolony complexes, despite some bacterial binding on the apatitic surface, whereas a strain defective in *gtfC* assembled a rudimentary EPS matrix with smaller

390 microcolonies (35). Therefore, the greater disruption of insoluble glucan synthesis
391 measured for the the Δ*yidC2* compared to the Δ*yidC1* strain is consistent with the
392 differences in biofilm architecture observed between these two mutants. In preliminary
393 RNAseq experiments comparing global gene expression of the *yidC* mutants to that of
394 wild type, the Δ*yidC2* mutant demonstrated 320 differentially expressed (DE) genes
395 including greater than 4-fold decreased expression of both *gtfB* and *gtfC* (Palmer
396 unpublished). In contrast, and consistent with its less severe phenotype, the Δ*yidC1*
397 mutant had very few DE genes compared to wild-type.
398 Interestingly, alterations in EPS composition stemming from *yidC1* and *yidC2*
399 deletion influenced fundamental biophysical properties of *S. mutans* biofilms, but in
400 different ways. Less insoluble EPS in the Δ*yidC2* mutant biofilm likely resulted in
401 elevation of stiffness (elastic modulus, *E*) (Figure 7), while the biofilm was more
402 susceptible to shearing, compared with intact wild-type biofilm. Bacterial and EPS
403 density may determine the mechanical properties of biofilm as bacteria are stiffer than a
404 polymer matrix (48). Thus, it is possible that a relatively high cell density (bacterial
405 volume fraction) in the Δ*yidC2* mutant biofilm contributes to the enhanced stiffness of
406 the biofilm observed in our compression experiments. Furthermore, elastic material can
407 absorb stress energy through deformation. Therefore, the decreased insoluble EPS in
408 the Δ*yidC2* mutant likely reduced the elasticity of the biofilm. Insufficient EPS in biofilms
409 may diminish cohesion between bacteria within biofilms (36, 38), such that during shear
410 stress the biofilm fails along sliding planes and allows for more sloughing of cells.
411 Indeed, the Δ*yidC2* mutant biofilm was more easily detached when subjected to shear
412 force (Figure 8). These results are consistent with the biochemical test results, in that

structural integrity of *S. mutans* biofilms is determined by the EPS matrix composition, whereas increased mechanical stability is correlated with increased levels of insoluble **α**-1,3-glucan produced by GtfB and GtfC (38). It is important to note that in our experiments biofilms were grown under static conditions, and it is possible that results would differ if the biofilms were grown in the presence of shear force.

Taken together, our current results demonstrate that *S. mutans* YidC1 and YidC2 contribute to cell wall biosynthesis and cell morphology, as well as to biofilm development and stability. The changes in the proportions of soluble/insoluble glucans produced by the *yidC* mutants influenced the structural integrity of the biofilm EPS matrix produced by *S. mutans* thus impacting optimal biofilm development and attachment, which likely contributed to the varying degrees of reduced virulence observed in a rat caries model (25). The biofilm EPS matrix produced by the Δ*yidC2* mutant, in particular, was affected in such a way so as to increase susceptibility to shear stress and to facilitate biofilm removal. Thus, targeting *S. mutans* YidCs, especially YidC2, may be an effective adjunctive treatment to disrupt cariogenic biofilms.

Materials and Methods

Bacterial strains

Streptococcus mutans UA159 (ATCC 700610; serotype C) came from the laboratory stocks of R. A. Burne, at the University of Florida. *S. mutans* UA159, and derivatives, were routinely grown in Brain Heart Infusion broth (BHI, BD Bacto) at 37°C in a 5% CO_2 environment, unless otherwise indicated below. For biofilms used in CLSM, biochemical, Gtf activity and mechanical stability assays, *S. mutans* UA159 and *yidC*

436 mutant strains were grown in ultra-filtered (10 kDa molecular-weight cut-off membrane;
437 Prep/ Scale, Millipore, MA) buffered tryptone-yeast extract broth (UFTYE; 2.5% tryptone
438 and 1.5% yeast extract, pH 7.0) with 1% glucose (37˚C, 5% CO_2) prior to use. For SIM
439 confocal experiments, cells were grown in Todd Hewitt Yeast Extract (THYE, 0.3%
440 yeast extract). Where appropriate, spectinomycin 1 mg ml^{-1}, or erythromycin 10 µg ml^{-1}
441 was added to broth or agar.

442 **Construction of Δ*yidC1* or Δ*yidC2* mutant**

443 Allelic replacement was used to replace the *yidC1* or *yidC2* genes with a
444 promoterless non-polar antibiotic marker in parent strain *S. mutans* UA159, without
445 disrupting expression of the surrounding genes and allowed expression of the antibiotic
446 marker from the endogenous *yidC1/2* promoter. The sequence of primers used to
447 construct the mutants are in Table 1. For the Δ*yidC1::Sp*^{r} (Smu.337) strain a 450 bp
448 upstream DNA fragment was amplified by PCR with primers SP62F and SP62R-SOE,
449 the *aad9* gene for Spectinomycin resistance was amplified by PCR from pDL278 (49)
450 using SP63F-SOE and SP63R-SOE, and a 437 bp downstream DNA segment was
451 amplified with primers SP64F-SOE and SP64R. PCR products were gel purified
452 (QIAquick gel extraction kit, Qiagen). Primers with a SOE designation (splice overlap
453 extension) contain 9 bp overlapping sequences with the adjacent primer to facilitate
454 joining of fragments using the 5'- and 3' terminal primers. Splice overlap extension
455 (SOE) PCR was performed with 50 ng of each fragment and primers SP62F and SP64R
456 for Δ*yidC1::Sp*^{r}, as described in (25). The final PCR product was used to transform
457 parent *S. mutans* strain UA159, with selection on BHI-Spec agar plates. The
458 Δ*yidC2::Erm*^{r} knockout construct was made using the same approach with primers

SP56F and SP56R-SOE used to amplify a 382 bp upstream region, SP57F-SOE and SP57R-SOE to amplify the Erythromycin resistance gene from pJL105, and SP58F-SOE and SP58R to amplify 393 bp downstream of *yidC2.* The three fragments were joined in an SOE PCR reaction using SP56F and SP58R, followed by natural transformation into the parent *S. mutans* strain UA159 and selection on BHI-Erm plates.

Construction of complemented *yidC2* mutant (conditional expression strain)

To generate a *yidC2* conditional expression strain for complementation experiments, *yidC2* was inserted into the pZX10 Xyl-S2 plasmid under the control of a xylose-inducible promoter (50). To generate the plasmid construct, the expression vector backbone pZX10 and the *yidC2* gene were amplified by PCR with primer pairs pZX10F-yidC2F and pZX10R-yidC2R and yidC2F-pZX10F and yidC2R-pZx10R, respectively. Complementary ends between the two amplicons facilitated the generation of concatemers using prolonged overlap extension PCR (POE-PCR) as described in (51). The resulting POE-PCR mixture was used to directly transform UA159 by natural transformation and transformants were selected on BHI containing spectinomycin generating a strain containing the resulting plasmid. The *yidC2* gene was then deleted from the chromosome as described above (Figure S1). Western blot with anti-YidC2 C-terminal antibody as described in (25) was used to verify tunable expression in various medias (Figure S1B). For growth experiments where *yidC2* expression was desired, 1% xylose was added to media along with Spectinomycin in order to maintain the plasmid.

Microscopic analysis

Gram-stains were performed on overnight cultures grown in BM media supplemented with 20 mM glucose (52), following manufacturer's protocol (Protocol Stabilized Gram Stain set, Fisher Scientific). Cells were mounted on glass slides with glass coverslips using Depex Mounting media (Electron Microscopy Sciences) and visualized using a 100 X oil emersion objective on an Olympus BX43. Images were taken using an Olympus DP72 camera, and scale bars added using CellSense Software (Olympus) or calibrated images in ImageJ (v. 2.0.0).

Electron microscopy

For SEM and TEM experiments, cells were grown overnight in 500 mL BM media supplemented with 20 mM glucose (52). Cells were pelleted at (3,500 g, 10 min, 4°C) and washed 3 times with 1 X phosphate buffered saline (PBS). Cells were then fixed for 30 min in a buffer containing 2.5% glutaraldehyde [0.1M phosphate buffer pH 7.4 (PB), and 0.1M sucrose] and washed 3 times in PB. The fixed samples were then processed by the Campus Microscopy & Imaging Facility (CMIF) at The Ohio State University using the following protocol. Cells were briefly suspended in warm 2% agarose, and pelleted before agar set, and chilled on ice for 10 min. Cells were post-fixed for 1 hr in 1% osmium tetroxide in PB, followed by 3 rinses for 5 min each in PB. Samples were dehydrated in successive 10 min exposures to increasing concentrations of ethanol: 50% ethanol, 70% ethanol, 80% ethanol, and then 5 min in 95% ethanol, followed by an additional 5 min in fresh 95% ethanol. The final dehydration step was performed in 100% ethanol (new bottle) with 3 changes within 15 min. The dehydrated samples were treated with propylene oxide for 10 min, followed by 1 hr treatment in 1:1 propylene oxide/resin, 1:2 propylene oxide/resin-overnight, and 100% Epon resin, with 2 changes

over 2-6 hr. Samples were embedded in fresh Epon resin and polymerized overnight at 60°C, and sectioned into ultra-thin sections (70 nm) on a Leica UC6 ultramicrotome using a Diatome diamond knife. Grids were post-stained with 1% uranyl acetate and Reynold's lead citrate buffers and then imaged on an FEI Tecnai G2 Spirit TEM, operating at 80 keV and micrographs collected in the range of 4,000 - 100,000 X magnification. Results shown are of representative images. The analyze feature in ImageJ (v. 2.0.0) was used to measure cell wall thickness and cell diameter. Images were calibrated based on the number of pixels in the scale bar. For cell wall thickness, 3 separate measurements were averaged together for each cell, with a minimum of 9 cells measured per strain. For cell diameter, measurements were taken across the middle of each cell at the narrowest point. A minimum of 6 cells were compared for each strain. One-Way ANOVA with Dunnett's post hoc test was used to determine significant differences between mutant and wild-type strains.

Super resolution structured Illumination Microscopy (SIM).

Cells were grown in THYE (0.3% yeast extract, pH 7.4) media over night at 37 °C. The following morning ON cultures were diluted 1:200 in fresh media at either pH 7.4 or pH 5. Once cells reached an OD_{600} ~ 0.5, fluorescent Vancomycin [2 µg ml^{-1}] was added to the cultures, incubated for 10 min and then washed twice in PBS. An aliquot of cells (~ 5 µl) was transferred to an agarose pad (3% w/v) and covered with a pre-cleaned cover slip (#1.5). Imaging was performed within 5-10 minutes after washing. Structured Illumination Microscopy (SIM) imaging was preformed as previously described (53, 54). In brief, images were acquired on a Zeiss ELYRA PS1 (pco.edge sCMOS camera) with a final pixel size of 50 nm, equipped with a 100X

526 1.46NA plan Apo oil immersion objective. Individual images were acquired with an
527 acquisition time of 300 ms per image (a total of 15 images were acquired per SIM image
528 reconstruction) and subsequently reconstructed from the raw data in the ZEN2012
529 software. All imaging was performed at room temperature (~23-24 °C). Reconstructed
530 SIM images were transferred to ImageJ (Fiji) for analysis and figure preparation. The
531 cell diameter determination was performed using ImageJ (Fiji), and line scans were
532 manually drawn over the widest width of each measured cell, where 77-87 cells were
533 measured for each strain. Statistical analysis was carried out in Origin 9 Pro, with two-
534 tailed Student's t-test showing a significant difference between WT and Δ*yidC2* ($P < 0.0001$). Graphs were made using Adobe illustrator.

535

536 **Confocal laser scanning microscopy (CLSM)**

537 CLSM experiments were performed essentially as described in (35, 47). Briefly,
538 *S. mutans* and *yidC* mutants biofilms were formed on saliva-coated hydroxyapatite (sHA)
539 disc surfaces as detailed previously. Hydroxyapatite discs (1.25 cm in diameter, surface
540 area of 2.7 ± 0.2 cm^2, Clarkson, Chromatography Products, Inc., South Williamsport, PA)
541 were coated with filter-sterilized, clarified human whole saliva (47). Then, each sHA disc
542 was inoculated with 10^5 CFU of actively growing *S. mutans* or *yidC1/2* mutant cells per
543 mL in UFTYE medium containing 1% (w/v) sucrose, and grown at 37˚C with 5% CO_2 for
544 19 hr. EPS was labeled using 1 μM Alexa Fluor 647-dextran conjugate (10 kDa;
545 647/668 nm; Molecular Probes Inc.), while the bacteria cells were stained with 2.5 μM
546 SYTO 9 (485/498 nm; Molecular Probes Inc.). The imaging was performed using a
547 multi-photon Leica SP5 confocal microscope with 20 X (numerical aperture, 1.00) water
548 immersion objective. The excitation wavelength was 780 nm, and the emission

549 wavelength filter for SYTO 9 was a 495/540 OlyMPFEC1 filter, while the filter for Alexa
550 Fluor 647 was a HQ655/40M-2P filter. Confocal image stacks were generated by optical
551 sectioning at each selected position and the step size of z-series scanning was 2 μm
552 (47). Amira 5.4.1 software (Visage Imaging, San Diego, CA, USA) was used to create
553 3D renderings of biofilm architecture. The total biomass of bacterial cells, EPS and
554 diameter of microcolonies were quantified and analyzed using COMSTAT 2.0 and
555 ImageJ 1.44 (47).

556 **Glycosyltransferase activity**

557 Extracellular Gtf activity produced by planktonic cultures of *yidC* mutants and the
558 wild type was measured as described by Koo et al. with some modifications (55). Briefly,
559 *S. mutans* UA159 and *yidC* mutants were grown in UFTYE medium containing 1% (w/v)
560 glucose. Growth was assessed by optical density of the culture at 600 nm (OD_{600}).
561 Bacterial cells were harvested at the early-exponential (OD_{600} = 0.2) or mid-exponential
562 (OD_{600} = 0.5), and stationary phases (OD_{600} = 1.0) by centrifugation (10,000 *g*, 10 min,
563 4˚C), and supernatant fluids were collected for the analyses. Phenylmethylsufonyl
564 fluoride (0.1 mM, final concentration) was added to the supernatant as a protease
565 inhibitor, and the pH value was measured and adjusted to 6.8 if necessary. The Gtf
566 activity in supernatants was measured in terms of incorporation of [^{14}C-glucose] from
567 radiolabeled sucrose (New England Nuclear Research Products, Boston, MA) into
568 glucans in 4 hr at 37˚C as described elsewhere (56). One unit (U) of enzyme was
569 defined as the amount of enzyme needed to incorporate 1 μmol of glucose into glucan
570 over a 4 h reaction period. The cell-free supernatant was mixed with ([^{14}C]glucosyl)-
571 sucrose substrate (0.2 μCi/mL; 200 mM sucrose, 40 μM dextran T-10, 0.02% sodium

azide in Adsorption Buffer: 50 mM KCl, 0.35 mM K_2HPO_4, 0.65 mM KH_2PO_4, 1 mM $CaCl_2$, 0.1 mM $MgCl_2 \cdot 6H_2O$, pH 6.5) for 4 h at 37^{o}C to allow glucan synthesis. Insoluble glucans were collected after centrifugation (13,400 g, 4˚C, 10 min) and washed three times with water. Soluble glucans were precipitated with ethanol (final concentration: 70%) for 18 h at -20 ˚C.The amount of radiolabeled insoluble and soluble glucans were quantified by means of scintillation counting. Data were shown as fold change of Gtf activity in comparison to the wild type. Statistical differences were determined by One-way ANOVA with Dunnett's post hoc test.

Biochemical assays

The biofilm was homogenized via water bath sonication followed by probe sonication (30 s pulse at an output of 7W; Branson Sonifier 150, Branson Ultrasonics, Danbury, CT). The homogenized biofilm suspension was centrifuged at 5,500 *g*, 4°C, for 10 min, and pellet was washed twice with water. The pellet and all of the supernatants were retrieved, and the amount of water soluble and insoluble EPS in the biofilm were extracted and quantified via established colorimetric assays as detailed previously (57-59). Briefly, the supernatants were pooled and 3 volumes of cold ethanol were added, and the resulting precipitate was collected. The precipitate, or water soluble polysaccharide, was collected by centrifugation, washed with ice-cold 75% (v/v) ethanol three times and dried in a SpeedVac concentrator prior to colorimetric assay. In parallel, the biofilm pellet, after washing, was dried and weighed to determine the dry-weight biomass. The insoluble EPS was extracted using 1 N NaOH (1 mg of biofilm dry weight per 0.3 mL of 1 N NaOH), and the extract was precipitated with three volumes of cold ethanol and dried in a SpeedVac concentrator. The soluble and insoluble EPS

were resuspended in water and NaOH, respectively, and the amount of polysaccharides were measured using the phenol-sulfuric method with glucose as standard.

Rheometry – indentation - displacement assay

Biofilms were grown for 96 hr in 35 x 10 mm Falcon petri dishes on hydroxyapatite discs (1.25 cm in diameter, surface area of 2.7 ± 0.2 cm^2, Clarkson, Chromatography Products, Inc., South Williamsport, PA) in TYE media (2.5% tryptone, 1.5% yeast extract, 1% sucrose, pH 7.0) with daily media exchanges. Indentation/compression tests were performed using a Discovery Hybrid Rheometer-2 (HR-2) with a temperature controlled Peltier plate (25˚C) connected to a heat exchanger (TA Instruments). A normal force was applied using 8 mm Smart Swap geometry with an approach of 1 µm/s. The elastic modulus (*E*) of each biofilm was calculated based on the early, linear, part of the force-displacement curve, where the geometry first came into contact with the biofilm using the formula $E = slope*(1-v^2)/2r$ (60), where r = 4 mm (radius of geometry), and the Poisson's ratio (v) was assumed to be 0.5. The assay was repeated two times and results represent three biological replicates for each strain.

Mechanical stability of biofilm - detachment assay

The mechanical stability of biofilms formed by *S. mutans* and *yidC* mutants were compared using a custom built device as described by Hwang et al (38). Briefly, 43 hr biofilms formed on sHA were placed in the disk holders of the device, and then exposed to constant shear stress of 1.78 N/m^2 for 10 min. The duration of 10 min of shearing was determined to have reached a steady state of biofilm removal based on our previous study (38). The amount of biofilm dry-weight (biomass) before and after

application of shear stress was determined and the corresponding confocal images were obtained and analyzed.

Statistical Analysis

Unless otherwise indicated, Student's *t*-test was used to determine significant differences between wildtype samples and the *ΔyidC1* or *ΔyidC2* mutants.

Acknowledgements

We would like to thank Dr. Erin Gloag for her assistance with the Rheometry experiments. Also, we would like to thank Dr. Justin Merritt for sharing the conditional expression system, pZX10 Xyl-S2 used to make a complemented *yidC2* mutant. EM micrographs presented in this report were generated using the instruments and services at the Campus Microscopy and Imaging Facility, The Ohio State University. This facility is supported in part by grant P30 CA016058, National Cancer Institute, Bethesda, MD. This work was supported by NIH NIDCR award DE023833 (SRP) and NIH NIDCR DE008007(LJB). Authors declare no conflicts of interests.

References

1. **Marsh PD**. 2004. Dental plaque as a microbial biofilm. Caries Res **38**:204–211.
2. **Jakubovics NS**. 2015. Intermicrobial interactions as a driver for community composition and stratification of oral biofilms. J Mol Biol **427**:3662–3675.
3. **Loesche WJ**. 1986. Role of *Streptococcus mutans* in human dental decay. Microbiol Rev **50**:353–380.
4. **Takahashi N**, **Nyvad B**. 2011. The role of bacteria in the caries process: ecological perspectives. J Dent Res **90**:294–303.

5. **Bowen WH**, **Koo H**. 2011. Biology of *Streptococcus mutans*-derived glucosyltransferases: role in extracellular matrix formation of cariogenic biofilms. Caries Res **45**:69–86.

6. **Koo H**, **Falsetta ML**, **Klein MI**. 2013. The exopolysaccharide matrix: A virulence determinant of cariogenic biofilm. J Dent Res **92**:1065–1073.

7. **Ohle von C**, **Gieseke A**, **Nistico L**, **Decker EM**, **DeBeer D**, **Stoodley P**. 2010. Real-time microsensor measurement of local metabolic activities in *ex vivo* dental biofilms exposed to sucrose and treated with chlorhexidine. Appl Environ Microbiol **76**:2326–2334.

8. **Marsh PD**. 2003. Are dental diseases examples of ecological catastrophes? Microbiology (Reading, Engl) **149**:279–294.

9. **Schneewind O**, **Missiakas DM**. 2012. Protein secretion and surface display in Gram-positive bacteria. Philos Trans R SocB **367**:1123–1139.

10. **Banas JA**, **Vickerman MM**. 2003. Glucan-binding Proteins of the Oral Streptococci. Crit Rev Oral Biol Med **14**:89–99.

11. **Plessis du DJF**, **Nouwen N**, **Driessen AJM**. 2011. The Sec translocase. Biochim Biophys Acta **1808**:851–865.

12. **Akopian D**, **Shen K**, **Zhang X**, **Shan S-O**. 2013. Signal recognition particle: an essential protein-targeting machine. Annu Rev Biochem **82**:693–721.

13. **Park E**, **Rapoport TA**. 2012. Mechanisms of Sec61/SecY-mediated protein translocation across membranes. Annu Rev Biophys **41**:21–40.

14. **Calo D**, **Eichler J**. 2011. Crossing the membrane in Archaea, the third domain of life. BBA - Biomembranes **1808**:885–891.

15. **Yuan J**, **Zweers JC**, **van Dijl JM**, **Dalbey RE**. 2009. Protein transport across and into cell membranes in bacteria and archaea. Cell Mol Life Sci **67**:179–199.

16. **Hasona A**, **Crowley PJ**, **Levesque CM**, **Mair RW**, **Cvitkovitch DG**, **Bleiweis AS**, **Brady LJ**. 2005. Streptococcal viability and diminished stress tolerance in mutants lacking the signal recognition particle pathway or YidC2. PNAS **102**:17466–17471.

17. **Williams ML**, **Crowley PJ**, **Hasona A**, **Brady LJ**. 2014. YlxM is a newly identified accessory protein that influences the function of signal recognition particle pathway components in *Streptococcus mutans*. J Bacteriol **196**:2043–2052.

18. **Lewis NE**, **Brady LJ**. 2014. Breaking the bacterial protein targeting and translocation model: oral organisms as a case in point. Mol Oral Microbiol **30**:186–197.

19. **Rosch JW**, **Vega LA**, **Beyer JM**, **Lin A**, **Caparon MG**. 2008. The signal recognition particle pathway is required for virulence in *Streptococcus pyogenes*. Infect Immun **76**:2612–2619.

20. **Hennon SW**, **Soman R**, **Zhu L**, **Dalbey RE**. 2015. YidC/Alb3/Oxa1 Family of Insertases. J Biol Chem **290**:14866–14874.

21. **Dalbey RE**, **Wang P**, **Kuhn A**. 2011. Assembly of bacterial inner membrane proteins. Annu Rev Biochem **80**:161–187.

22. **Steinberg R**, **Knüpffer L**, **Origi A**, **Asti R**, **Koch H-G**. 2018. Co-translational protein targeting in bacteria. FEMS Microbiol Lett **365**:5564.

23. **Dalbey RE**, **Kuhn A**, **Zhu L**, **Kiefer D**. 2014. The membrane insertase YidC. Biochim Biophys Acta **1843**:1489–1496.

24. **de Sousa Borges A**, **de Keyzer J**, **Driessen AJM**, **Scheffers D-J**. 2015. The *Escherichia coli* membrane protein insertase YidC assists in the biogenesis of penicillin binding proteins. J Bacteriol **197**:1444–1450.

25. **Palmer SR**, **Crowley PJ**, **Oli MW**, **Ruelf MA**, **Michalek SM**, **Brady LJ**. 2012. YidC1 and YidC2 are functionally distinct proteins involved in protein secretion, biofilm formation and cariogenicity of *Streptococcus mutans*. Microbiology **158**:1702–1712.

26. **Tjalsma H**, **Bron S**, **van Dijl JM**. 2003. Complementary impact of paralogous Oxa1-like proteins of *Bacillus subtilis* on post-translocational stages in protein secretion. J Biol Chem **278**:15622–15632.

27. **Hofbauer B**, **Vomacka J**, **Stahl M**, **Korotkov VS**, **Jennings MC**, **Wuest WM**, **Sieber SA**. 2018. Dual inhibitor of *Staphylococcus aureus* virulence and biofilm attenuates expression of major toxins and adhesins. Biochemistry **57**:1814–1820.

28. **Dong Y**, **Palmer SR**, **Hasona A**, **Nagamori S**, **Kaback HR**, **Dalbey RE**, **Brady LJ**. 2008. Functional overlap but lack of complete cross-complementation of *Streptococcus mutans* and *Escherichia coli* YidC orthologs. J Bacteriol **190**:2458–2469.

29. **Saller MJ**, **Wu ZC**, **de Keyzer J**, **Driessen AJM**. 2012. The YidC/Oxa1/Alb3 protein family: common principles and distinct features. Biol Chem **393**.

30. **Kumazaki K**, **Chiba S**, **Takemoto M**, **Furukawa A**, **Nishiyama K-I**, **Sugano Y**, **Mori T**, **Dohmae N**, **Hirata K**, **Nakada-Nakura Y**, **Maturana AD**, **Tanaka Y**, **Mori H**, **Sugita Y**, **Arisaka F**, **Ito K**, **Ishitani R**, **Tsukazaki T**, **Nureki O**. 2014. Structural basis of Sec-independent membrane protein insertion by YidC. Nature **509**:516–520.

31. **Wu ZC**, **de Keyzer J**, **Berrelkamp-Lahpor GA**, **Driessen AJM**. 2013. Interaction

of *Streptococcus mutans* YidC1 and YidC2 with translating and nontranslating ribosomes. J Bacteriol **195**:4545–4551.

32. **Shankar M**, **Mohapatra SS**, **Biswas S**, **Biswas I**. 2015. Gene regulation by the LiaSR two-component system in *Streptococcus mutans*. PLoS ONE **10**:e0128083.

33. **Samuelson JC**, **Chen M**, **Jiang F**, **Moller I**, **Wiedmann M**, **Kuhn A**, **Phillips GJ**, **Dalbey RE**. 2000. YidC mediates membrane protein insertion in bacteria. Nature **406**:637–641.

34. **Klein MI**, **Hwang G**, **Santos PHS**, **Campanella OH**, **Koo H**. 2015. *Streptococcus mutans*-derived extracellular matrix in cariogenic oral biofilms. Front Cell Infect Microbiol **5**:10.

35. **Koo H**, **Xiao J**, **Klein MI**, **Jeon JG**. 2010. Exopolysaccharides produced by *Streptococcus mutans* glucosyltransferases modulate the establishment of microcolonies within multispecies biofilms. J Bacteriol **192**:3024–3032.

36. **Klapper I**, **Rupp CJ**, **Cargo R**, **Purvedorj B**, **Stoodley P**. 2002. Viscoelastic fluid description of bacterial biofilm material properties. Biotechnol Bioeng **80**:289–296.

37. **Vinogradov AM**, **Winston M**, **Rupp CJ**, **Stoodley P**. 2004. Rheology of biofilms formed from the dental plaque pathogen *Streptococcus mutans*. Biofilms **1**:49–56.

38. **Hwang G**, **Klein MI**, **Koo H**. 2014. Analysis of the mechanical stability and surface detachment of mature *Streptococcus mutans* biofilms by applying a range of external shear forces. Biofouling **30**:1079–1091.

39. **Crowley PJ**, **Brady LJ**. 2016. Evaluation of the effects of *Streptococcus mutans* chaperones and protein secretion machinery components on cell surface protein biogenesis, competence, and mutacin production. Mol Oral Microbiol **31**:59–77.

40. **Wang P**, **Kuhn A**, **Dalbey RE**. 2010. Global change of gene expression and cell physiology in YidC-depleted *Escherichia coli*. J Bacteriol **192**:2193–2209.

41. **Weiss DS**, **Chen JC**, **Ghigo JM**, **Boyd D**, **Beckwith J**. 1999. Localization of FtsI (PBP3) to the septal ring requires its membrane anchor, the Z ring, FtsA, FtsQ, and FtsL. J Bacteriol **181**:508–520.

42. **Pedersen LB**, **Angert ER**, **Setlow P**. 1999. Septal localization of penicillin-binding protein 1 in *Bacillus subtilis*. J Bacteriol **181**:3201–3211.

43. **Scheffers D-J**, **Errington J**. 2004. PBP1 is a component of the *Bacillus subtilis* cell division machinery. J Bacteriol **186**:5153–5156.

44. **Wen ZT**, **Bitoun JP**, **Liao S**. 2015. PBP1a-deficiency causes major defects in cell division, growth and biofilm formation by *Streptococcus mutans*. PLoS ONE

10:e0124319.

45. **Hanada N**, **Kuramitsu HK**. 1989. Isolation and characterization of the *Streptococcus mutans gtfD* gene, coding for primer-dependent soluble glucan synthesis. Infect Immun **57**:2079–2085.

46. **Silhavy TJ**, **Kahne D**, **Walker S**. 2010. The bacterial cell envelope. Cold Spring Harbor Perspectives in Biology **2**:a000414–a000414.

47. **Xiao J**, **Klein MI**, **Falsetta ML**, **Lu B**, **Delahunty CM**, **Yates JR**, **Heydorn A**, **Koo H**. 2012. The exopolysaccharide matrix modulates the interaction between 3D architecture and virulence of a mixed-species oral biofilm. PLoS Pathog **8**:e1002623–16.

48. **Gordon VD**, **Davis-Fields M**, **Kovach K**, **Rodesney CA**. 2017. Biofilms and mechanics: a review of experimental techniques and findings. J Phys D: Appl Phys **50**:1–12.

49. **LeBlanc DJ**, **Lee LN**, **Abu-Al-Jaibat A**. 1992. Molecular, genetic, and functional analysis of the basic replicon of pVA380-1, a plasmid of oral streptococcal origin. Plasmid **28**:130–145.

50. **Xie Z**, **Qi F**, **Merritt J**. 2013. Development of a tunable wide-range gene induction system useful for the study of Streptococcal toxin-antitoxin systems. Appl Environ Microbiol **79**:6375–6384.

51. **Xie Z**, **Okinaga T**, **Qi F**, **Zhang Z**, **Merritt J**. 2011. Cloning-independent and counterselectable markerless mutagenesis system in *Streptococcus mutans*. Appl Environ Microbiol **77**:8025–8033.

52. **Loo CY**, **Corliss DA**, **Ganeshkumar N**. 2000. *Streptococcus gordonii* Biofilm Formation: Identification of Genes that Code for Biofilm Phenotypes. J Bacteriol **182**:1374–1382.

53. **Söderström B**, **Mirzadeh K**, **Toddo S**, **Heijne von G**, **Skoglund U**, **Daley DO**. 2016. Coordinated disassembly of the divisome complex in *Escherichia coli*. Mol Microbiol **101**:425–438.

54. **Söderström B**, **Chan H**, **Shilling PJ**, **Skoglund U**, **Daley DO**. 2017. Spatial separation of FtsZ and FtsN during cell division. Mol Microbiol **107**:387–401.

55. **Koo H**, **Schobel B**, **Scott-Anne K**, **Watson G**, **Bowen WH**, **Cury JA**, **Rosalen PL**, **Park YK**. 2005. Apigenin and tt-farnesol with fluoride effects on *S. mutans* biofilms and dental caries. J Dent Res **84**:1016–1020.

56. **Koo H**, **Vacca Smith AM**, **Bowen WH**, **Rosalen PL**, **Cury JA**, **Park YK**. 2000. Effects of *Apis mellifera* propolis on the activities of streptococcal glucosyltransferases in solution and adsorbed onto saliva–coated hydroxyapatite.

784 Caries Res **34**:418–426.

785 57. **Koo H**, **Hayacibara MF**, **Schobel BD**, **Cury JA**, **Rosalen PL**, **Park YK**, **Vacca**
786 **Smith AM**, **Bowen WH**. 2003. Inhibition of *Streptococcus mutans* biofilm
787 accumulation and polysaccharide production by apigenin and *tt*-farnesol. J
788 Antimicrob Chemother **52**:782–789.

789 58. **Aparecido Cury J**, **Seils J**, **Koo H**. 2008. Isolation and purification of total RNA
790 from *Streptococcus mutans* in suspension cultures and biofilms. Braz Oral Res
791 **22**:216–222.

792 59. **Klein MI**, **DeBaz L**, **Agidi S**, **Lee H**, **Xie G**, **Lin AHM**, **Hamaker BR**, **Lemos JA**,
793 **Koo H**. 2010. Dynamics of *Streptococcus mutans* transcriptome in response to
794 starch and sucrose during biofilm development. PLoS ONE **5**:e13478.

795 60. **Timoshenko S**, **Goodier JN**. 1951. *Theory of Elasticity*. McGraw-Hill Book
796 Company, Inc.

797

798 **Figure legends**

799 **Figure 1. Gram stained and SEM images of *S. mutans* wild type and *yidC1/2***

800 **mutants.** A) Gram-stain results of WT *S. mutans* UA159, *yidC1* and *yidC2* mutants

801 visualized with 100 X objective. Boxes indicate location of zoomed-in image in right

802 panel. B) SEM images of indicated strains taken at 10,000 X and C) 40,000 X

803 magnification. Red arrows indicate aberrantly shaped cells with multiple division septa,

804 and yellow arrows indicate ovococci typical of *S. mutans*.

805 **Figure 2. Transmission electron micrographs of *S. mutans* wild type and *yidC1/2***

806 **mutants.** Representative micrographs of each strain taken at 4,000 X (A), 25,000 X (B),

807 and 60,000 X (C) magnification. D) Micrographs of cells with intact cell walls taken at

808 100,000 X magnification. E) Mean cell wall thickness of wild-type (WT) and *yidC*

809 mutants. F) Mean cell diameter of wild type and *yidC* mutant cells. Statistical differences

810 compared to WT are indicated by: * $P < 0.05$. Red arrows indicate abnormally shaped

dividing cells, and red bars indicate where measurements were taken for cell wall thickness.

Figure 3. Comparison of *de novo* cell wall synthesis measured by mid-cell localization of fluorescent Vancomycin. SIM images of cells grown either in pH 7.4 or pH 5.0 media: A) Wild-type *S. mutans*, B) Δ*yidC1,* and C) Δ*yidC2*. Panel D) shows the cell diameter (nm) measured in Fiji (imageJ) using calibrated images. Scale bars indicates 2 µm.

Figure 4. Growth phase dependent extracellular Gtf activity associated with *S. mutans* wild type and *yidC1/2* mutants. A) Insoluble glucans and B) soluble glucans produced by Gtf exoenzymes in culture supernatant derived from planktonically grown *S. mutans* strains. C) Insoluble glucans and D) soluble glucans produced by a complemented *yidC2* mutant strain grown with or without 1% xylose, where *yidC2* is only expressed in the presence of xylose. Statistical differences compared to wild type or in the presence of xylose, and are indicated by: * $P \leqslant 0.01$, ** $P \leqslant 0.001$, and *** $P \leqslant 0.0001$.

Figure 5. Composition of biofilms formed by *S. mutans* wild type and *yidC1/2* mutants in the presence of 1% sucrose. A) Total dry-weight of the resulting biofilms produced by the respective strains. B) Amount of insoluble, and C) soluble polysaccharides in the biofilms. Statistical differences are indicated by: * $P \leqslant 0.01$, ** $P \leqslant 0.001$, and *** $P \leqslant 0.0001$.

Figure 6. CLSM of *S. mutans* wild type and *yidC1/2* mutant biofilms. A)

Representative 3D images of biofilms formed by *S. mutans* UA159 (WT), *yidC1/2* mutant strains, or *yidC2* complemented mutant strain with or without xylose (inset), grown in the presence of 1% sucrose. All biofilms were heterogeneous and consisted of distinct microcolonies of cells separated by interstitial channels. Bacteria were stained with SYTO 9 (in green) and EPS was labeled with Alexa Fluor 647 (in red). B) Diameter of microcolonies. Statistical differences compared to WT are indicated by: * $P < 0.05$.

Figure 7. Biofilm thickness and elastic modulus of *S. mutans* wild type and *yidC1/2* mutants. The elastic modulus was calculated based an indentation/compression test performed on 96 hr biofilms formed in the presence of 1% sucrose on HA discs. A) Schematic of indentation/compression test performed on *S. mutans* biofilms. B) Resulting force-displacement curves from compression analysis. The portion of the curves where the slope was calculated to determine the elastic modulus is indicated by box. C) Biofilm thickness, and elastic modulus (mean ± 1 standard deviation, n=3) formed by wild type *S. mutans* and the *yidC* mutants are shown. Statistical differences compared to WT are indicated by: * $P < 0.003$.

Figure 8. Mechanical stability of biofilms under shear stress. A) Schematic diagram of shear-induced biofilm mechanical strength tester. B) The percentage of biomass lost after a shear stress of 1.78 N/m^2 was applied to biofilms. C) Bacteria and EPS biomass remaining on sHA surfaces after shear-stress was determined via COMSTAT. Statistical differences compared to WT are indicated by: * $P < 0.05$.

Table 1. Oligonucleotides used in this study

Primer name	Sequence[a]	Application
SP62F	GAGATTTTTGGCTTTTTCTCATTT	Δ*yidC1*::Sp^r
SP62R-SOE	CATAGTTGTGTGCTGCAACAGCTAATCCAA	Δ*yidC1*::Sp^r
SP63F-SOE	TTGCAGCACACAACTATGGATATAAAATAGGTA	Δ*yidC1*::Sp^r
SP63R-SOE	TTGTTCTCCGTTTCCACCATTTTTTCAATTTTT	Δ*yidC1*::Sp^r
SP64F-SOE	GGTGGAAACGGAGAACAAATCATGGTATTATT	Δ*yidC1*::Sp^r
SP64R	GCAGTGGCTGCCGATGTTTT	Δ*yidC1*::Sp^r
SP56F	CCAGAAGCACAAAGACAGCAAA	Δ*yidC2*::Erm^r
SP56R-SOE	CACTCCTTCGACGATTAACAACCATTGACTTTA	Δ*yidC2*::Erm^r
SP57F-SOE	GCTCTGTCTGAAGGAGTGATTACATGAACAAA	Δ*yidC2*::Erm^r
SP57R-SOE	GAAGAACTCCCCTTTAGTAACGTGTAACTTTCCA	Δ*yidC2*::Erm^r
SP58F-SOE	ACTAAAGGGGAGTTCTTCAACAAAACGTATTG	Δ*yidC2*::Erm^r
SP58R	GACAGTGATGCTGTTGCTAAA	Δ*yidC2*::Erm^r
pZX10F-YidC2F	CTGTTATCAACGGATCCACCTAACCGCCATAAACTGCCAGGCATC	pXyl- yidC2
pZX10R-YidC2R	GACGCTTGTAAATTTTTTTCACGATTACCTCCTTTGATTTAAGTGAACAAGT	pXyl- yidC2
YidC2F-pZX10F	ACTTGTTCACTTAAATCAAAGGAGGTAATCGTGAAAAAAATTTACAAGCGTC	pXyl-yidC2
YidC2R-pZX10R	GATGCCTGGCAGTTTATGGCGGTTAGGTGGATCCGTTGATAACAG	pXyl-yidC2

[a] Underlined sequence indicates location of overlapping segments for splice-overlap extension PCR or prolonged overlap extension PCR.

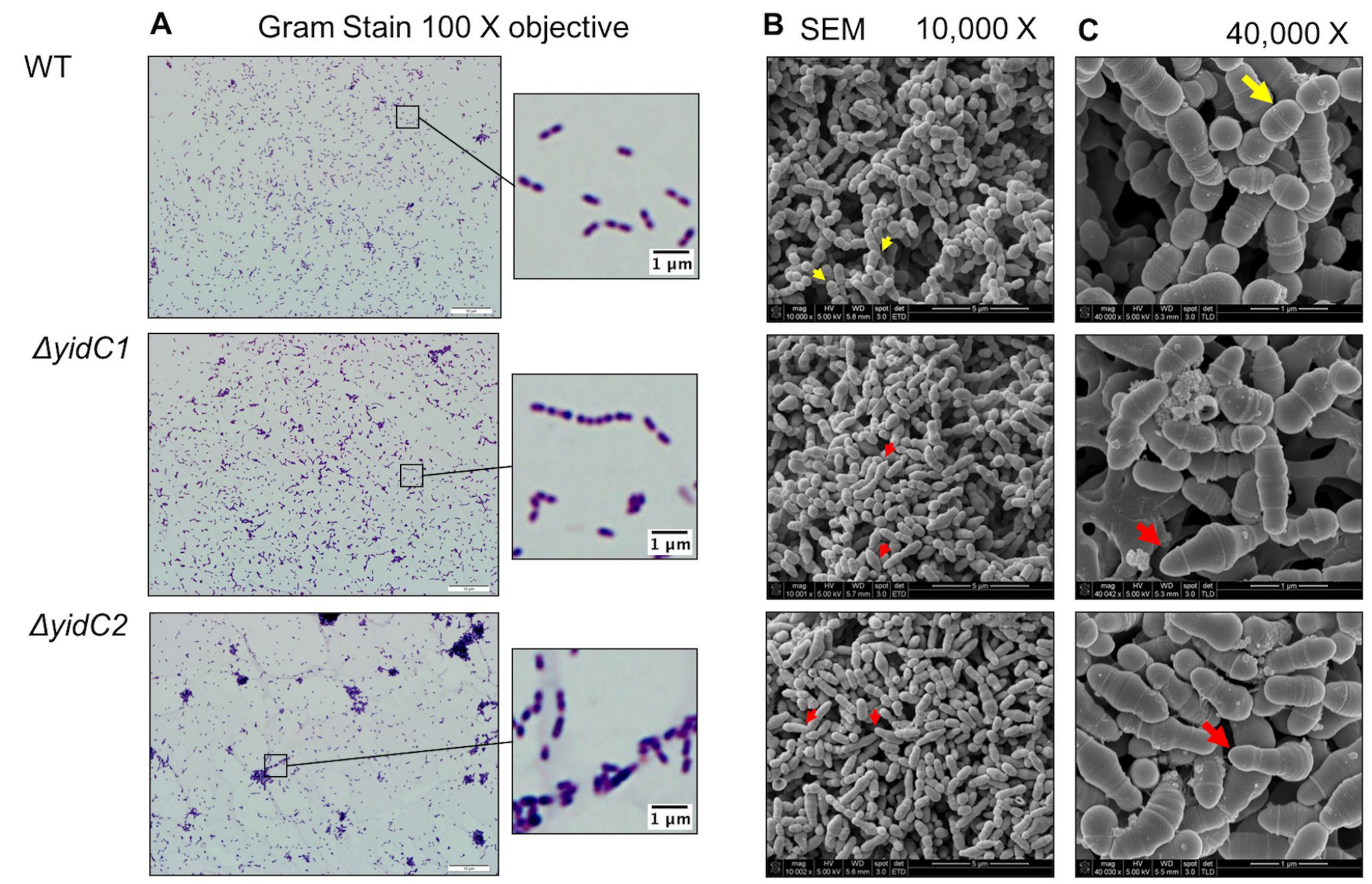
A
Gram Stain 100 X objective
B SEM 10,000 X
C 40,000 X
WT
ΔyidC1
ΔyidC2
1 µm
1 µm
1 µm

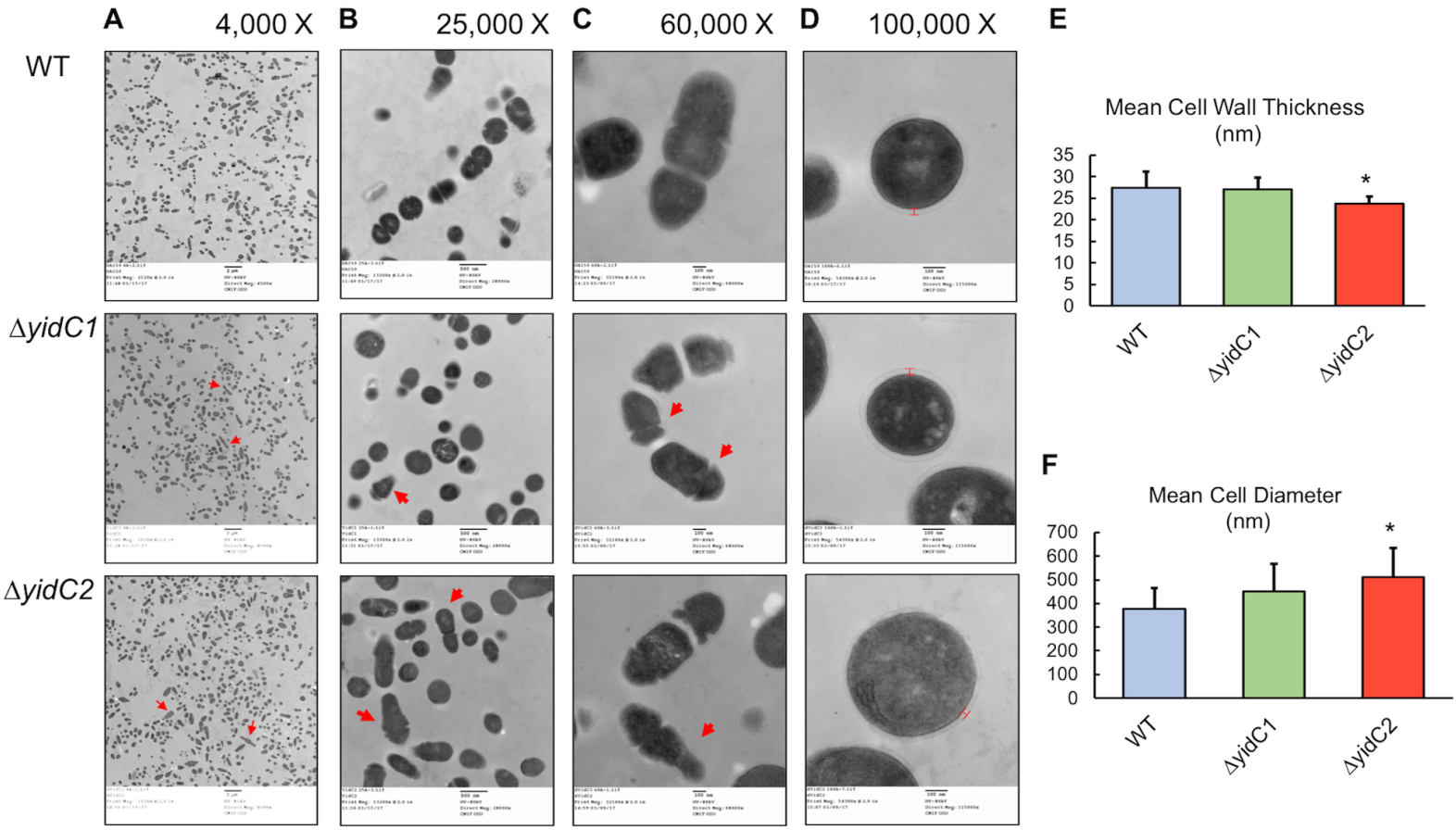
A
4,000 X
B
25,000 X
C
60,000 X
D
100,000 X
WT
ΔyidC1
ΔyidC2
E
Mean Cell Wall Thickness
(nm)
35
30
25
20
15
10
5
0
*
WT
ΔyidC1
ΔyidC2
F
Mean Cell Diameter
(nm)
700
600
500
400
300
200
100
0
*
WT
ΔyidC1
ΔyidC2

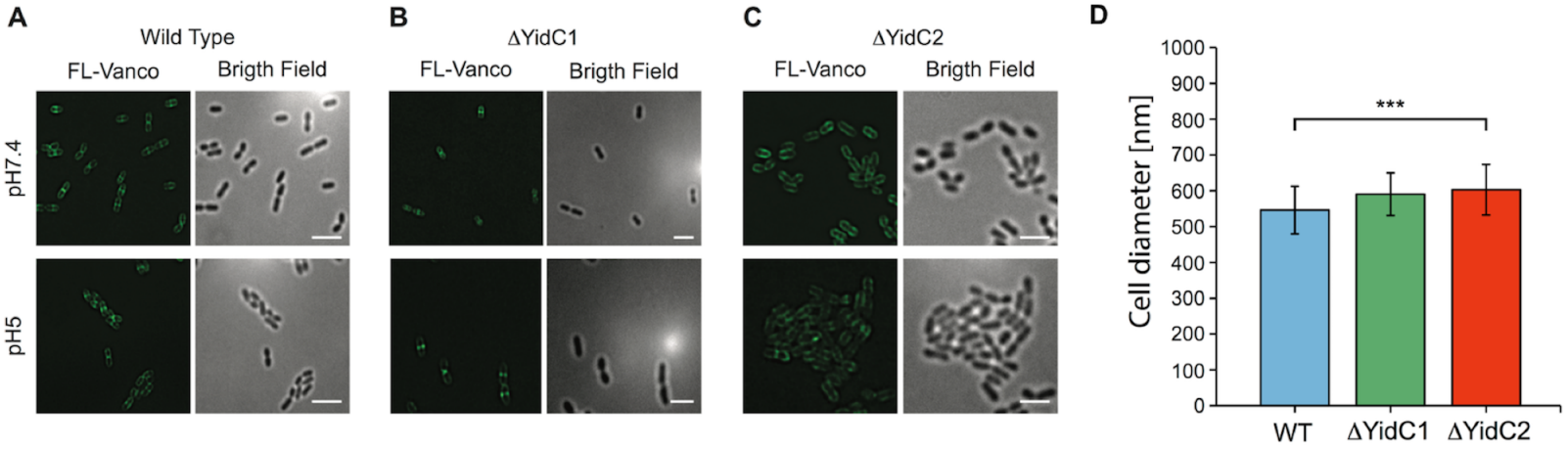
A
Wild Type
FL-Vanco
Brigth Field
pH7.4
pH5
B
ΔYidC1
FL-Vanco
Brigth Field
C
ΔYidC2
FL-Vanco
Brigth Field
D
Cell diameter [nm]
1000
900
800
700
600
500
400
300
200
100
0
***
WT
ΔYidC1
ΔYidC2

A

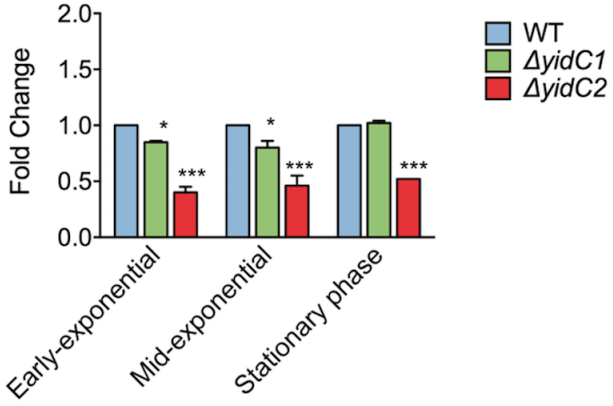
Gtf activity – insoluble glucans
Fold Change
2.0
1.5
1.0
0.5
0.0
*
***
*
***
***
Early-exponential
Mid-exponential
Stationary phase
WT
ΔyidC1
ΔyidC2

B

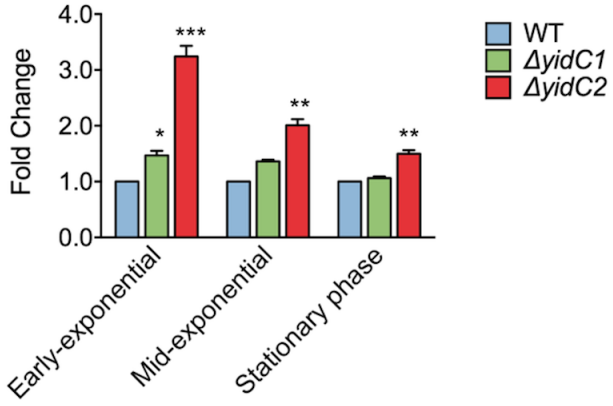
Gtf activity – soluble glucans
Fold Change
4.0
3.0
2.0
1.0
0.0
*
***
**
**
Early-exponential
Mid-exponential
Stationary phase
WT
ΔyidC1
ΔyidC2

C

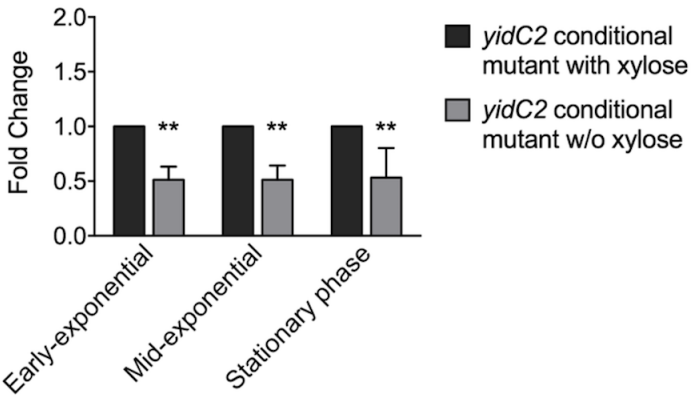
Gtf activity – insoluble glucans
(xylose-inducible yidC2 promoter)
Fold Change
2.0
1.5
1.0
0.5
0.0
**
**
**
Early-exponential
Mid-exponential
Stationary phase
yidC2 conditional mutant with xylose
yidC2 conditional mutant w/o xylose

D

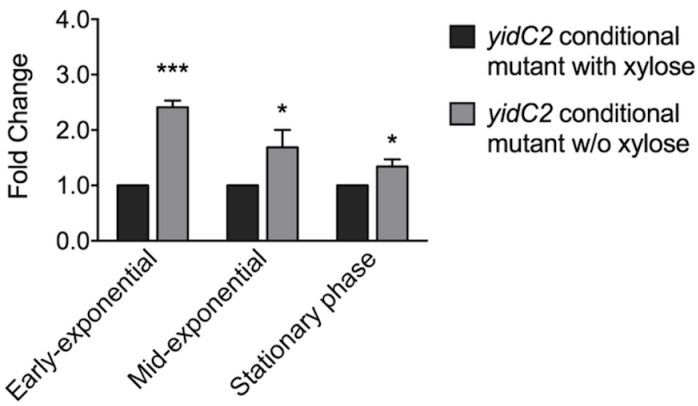
Gtf activity – soluble glucans
(xylose-inducible yidC2 promoter)
Fold Change
4.0
3.0
2.0
1.0
0.0
***
*
*
Early-exponential
Mid-exponential
Stationary phase
yidC2 conditional mutant with xylose
yidC2 conditional mutant w/o xylose

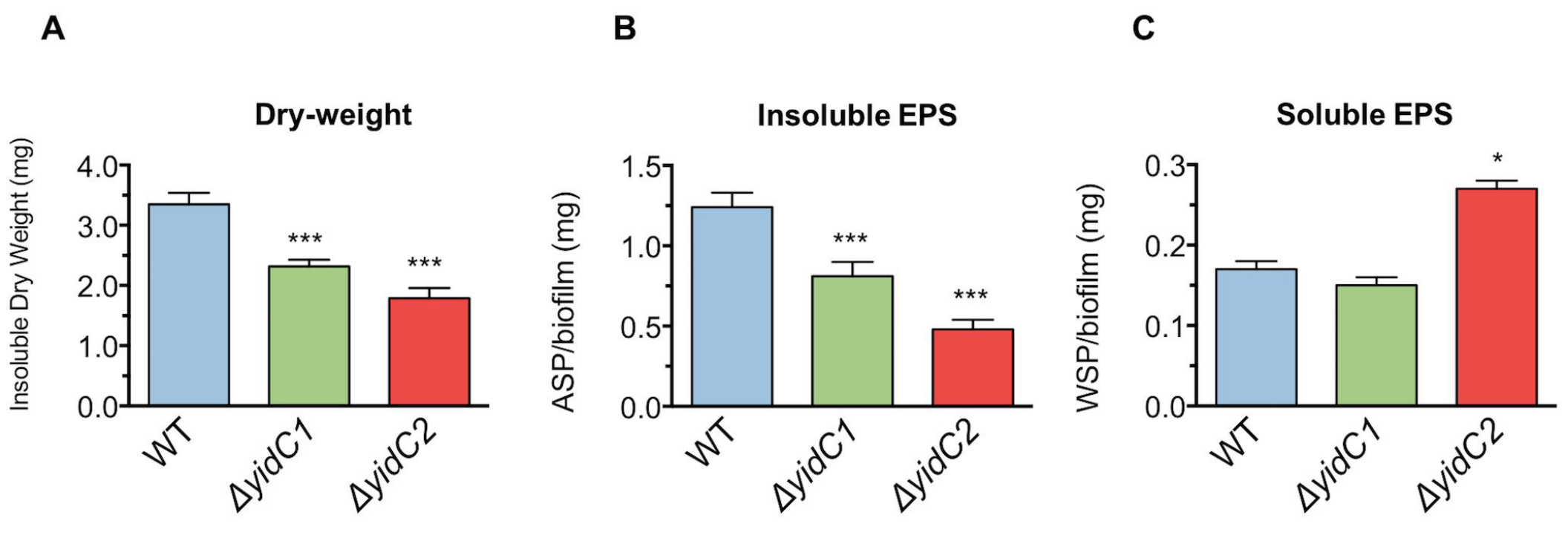
A
Dry-weight
Insoluble Dry Weight (mg)
4.0
3.0
2.0
1.0
0.0
***
***
WT
ΔyidC1
ΔyidC2
B
Insoluble EPS
ASP/biofilm (mg)
1.5
1.0
0.5
0.0
***
***
WT
ΔyidC1
ΔyidC2
C
Soluble EPS
WSP/biofilm (mg)
0.3
0.2
0.1
0.0
*
WT
ΔyidC1
ΔyidC2

A

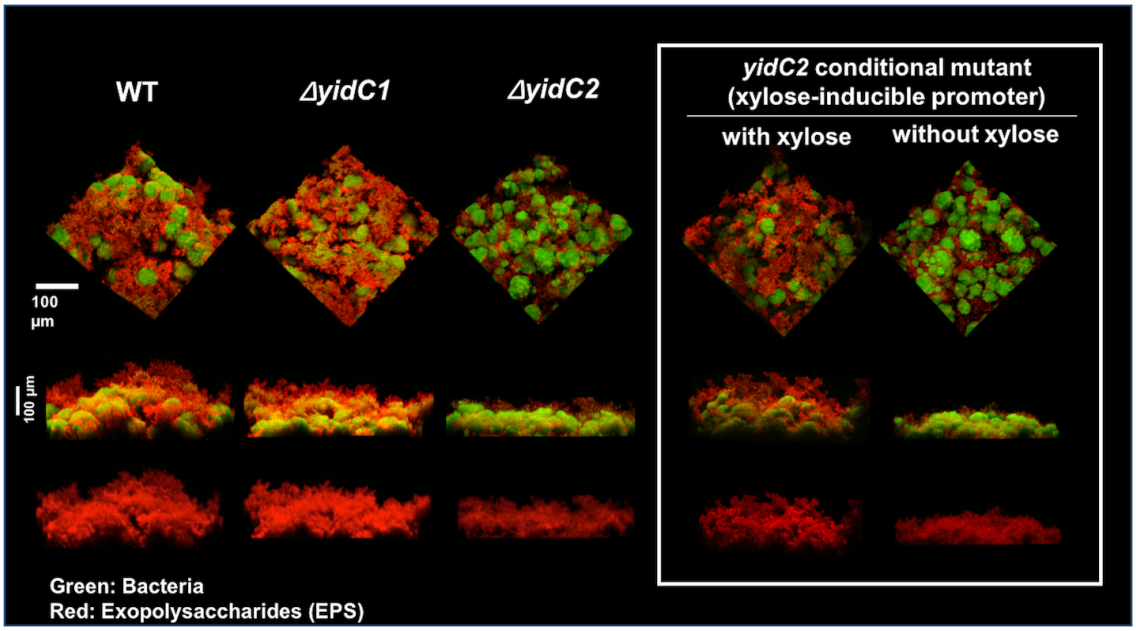
WT
ΔyidC1
ΔyidC2
yidC2 conditional mutant
(xylose-inducible promoter)
with xylose
without xylose
100 µm
100 µm
Green: Bacteria
Red: Exopolysaccharides (EPS)

B

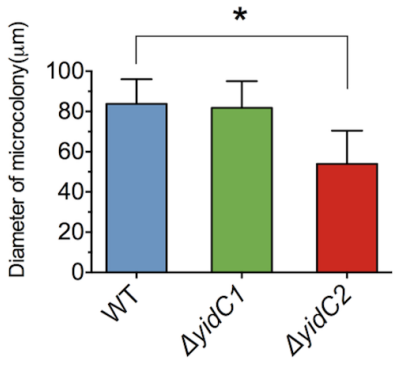
*
Diameter of microcolony(µm)
100
80
60
40
20
0
WT
ΔyidC1
ΔyidC2

A

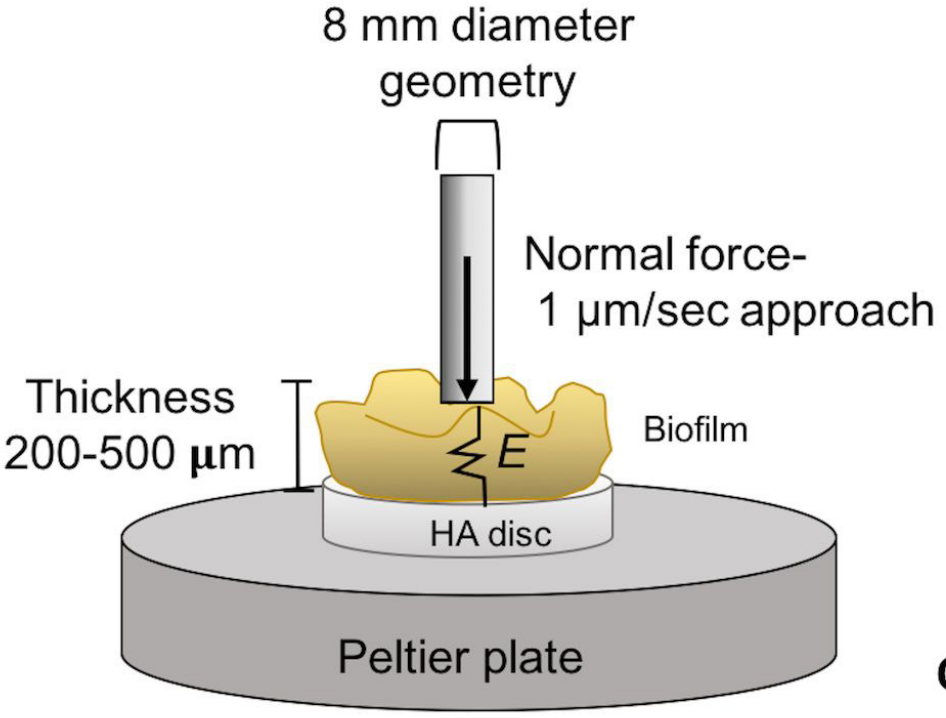

Elastic modulus

E = slope – $(1\text{-}v^2)/2*r$

r = 4 mm (radium of geometry), and
v = 0.5 (Poisson's ratio for rubber)

B

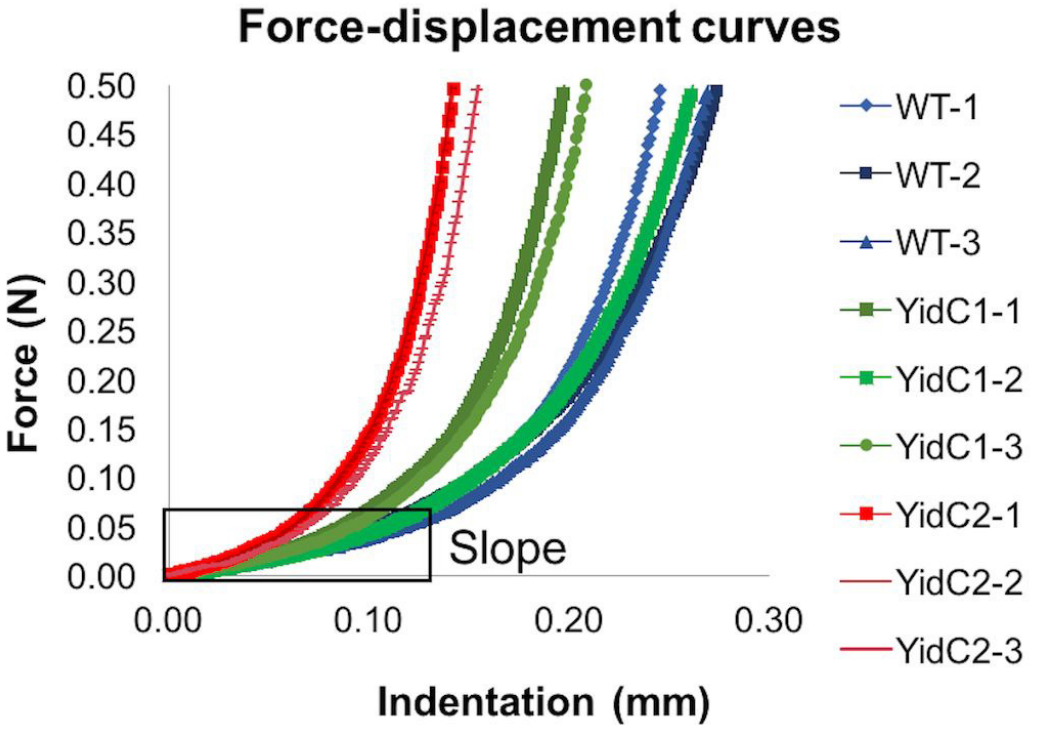

C

Strain	Mean ± SD Elastic modulus E = (kPa)	Mean ± SD Biofilm thickness (µM)
WT	42 ± 5	474 ± 171
Δ*yidC1*	47 ± 5	326 ± 42
Δ*yidC2*	70 ± 6 *	207 ± 22

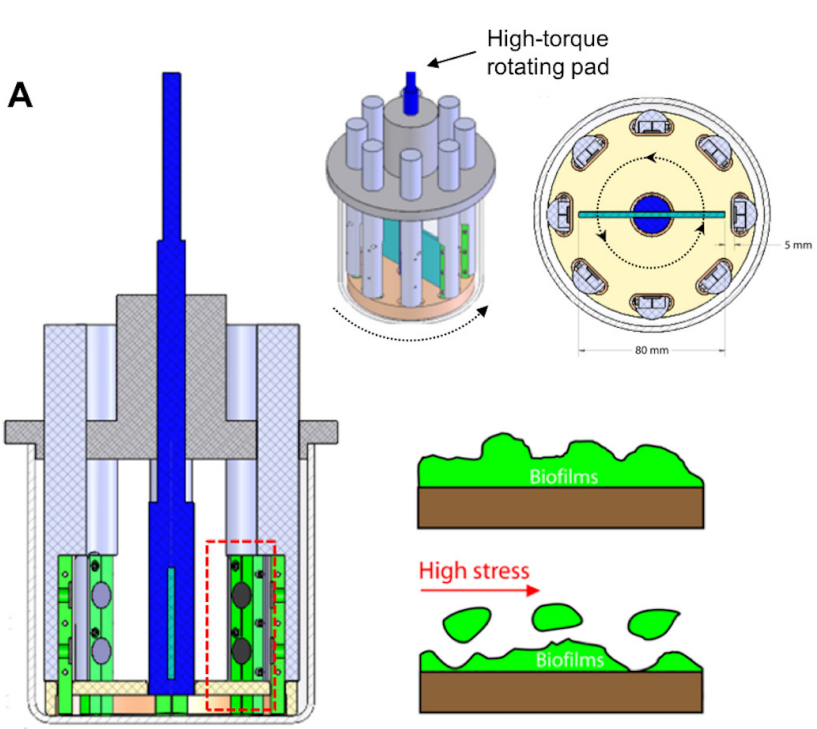
A
High-torque
rotating pad
5 mm
80 mm
Biofilms
High stress
Biofilms

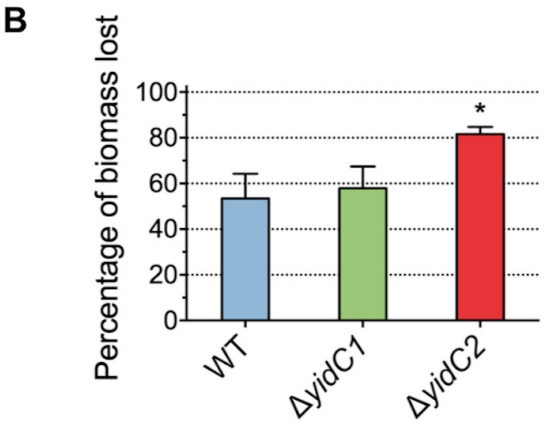
B
Percentage of biomass lost
100
80
60
40
20
0
*
WT
ΔyidC1
ΔyidC2

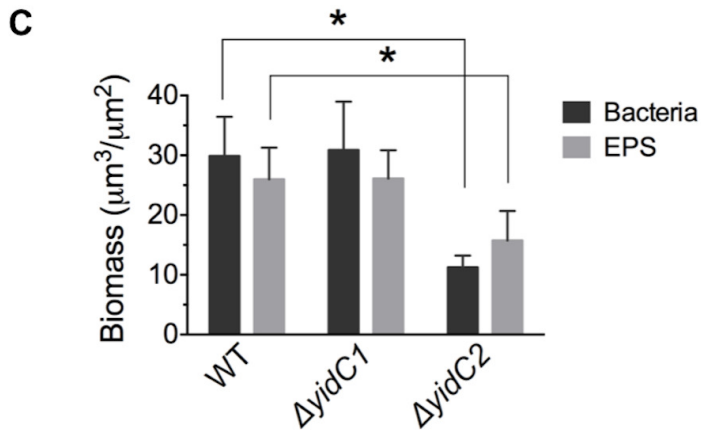
C
*
*
Biomass (μm³/μm²)
40
30
20
10
0
WT
ΔyidC1
ΔyidC2
Bacteria
EPS